Transactions of the 15th International Conference on
Structural Mechanics in Reactor Technology (SMiRT-15)
Seoul, Korea, August 15-20, 1999

Effects of Specimen Thickness and Microstructure on Near-Threshold Fatigue Crack Propagation in Ferritic Steels

Eung Seon Kim and In Sup Kim

Korea Advanced Institute of Science and Technology, Korea

ABSTRACT

In this study, the effect of specimen thickness on near-threshold fatigue crack propagation was investigated in consideration of microstructure. Fatigue tests were performed for three kinds of low carbon steel and one weld under a load ratio of 0.1 in room temperature air. The values of threshold were higher in thicker specimens regardless of the microstructures. As the effective grain size increased, the thickness effect became more pronounced. It was confirmed by the spheroidization of ferrite-pearlite microstructure that the pearlite influenced the threshold values in thick specimens by promoting tortuous asperities. The above effects of specimen thickness and microstructure were discussed on the basis of crack closure controlled by stress state at the crack tip.

INTRODUCTION

At near-threshold levels, several factors, such as microstructure, environment, and loading condition significantly affect fatigue crack propagation rates. The effects of these factors have been successfully explained by the concept of crack closure [1-5]. However, the inconsistency of threshold data is often observed depending on the specimen geometry. Especially, few investigations on the effect of specimen thickness have been performed in near-threshold region, and their conclusions are generally conflicting.

Two studies showed no significant differences over the thickness range of 5- 40mm [6, 7]. Radon et at. reported that near-threshold crack propagation rates increased and the values of threshold, ΔK_{th}, decreased as specimen thickness increased in BS4360-50D steel [8, 9]. However, the fracture surfaces were not observed and the reason for the thickness effect has not been clarified. Others showed higher values of measured threshold in thicker specimens [10, 11]. Romaniv et al. attributed the thickness effect to oxide-induced crack closure intensified by plastic constraint at the crack tip but ignored the contribution of roughness-induced crack closure by assuming that fracture micromechanisms were independent of specimen thickness [10]. Tokaji et al. discussed the effect of specimen thickness in the light of oxide-induced crack closure that was promoted by asperities [11]. However, they did not explain clearly the reason why the asperities were formed in low carbon steel (S10C) and not formed in high strength steel (HT60).

In order to clarify the above ambiguities, it is necessary to take into account the influence of microstructure in assessing the effect of specimen thickness on near-threshold fatigue

crack propagation. In this study, near-threshold crack propagation behaviors were investigated in three low carbon steels and one weld and discussed the effect of specimen thickness and microstructure on the basis of crack closure and stress state.

EXPERIMENTAL PROCEDURE

The materials used were SA106 Gr.C steel base and weld, SA508 Cl.3 steel, and 12% Cr steel. The SA106 Gr.C weld was fabricated using manual gas-tungsten-arc welding process. The chemical compositions are shown in Table 1. The spheroidization of the SA106 Gr.C steel base was performed at 690°C, which is about 15°C below the eutectoid temperature, for 340 hrs. The SA106 Gr.C steel base and weld were ferrite-pearlite microstructures. After the spheroidization, there was no change in the ferrite grain size, but the cementite plates in pearlites were converted to spheroidized particles as presented in Figure 1. The microstructures of the SA508 Cl.3 steel and the 12% Cr steel were tempered-bainite and tempered-martensite, respectively. The tensile properties at room temperature are presented in Table 2 with the microstructural characteristics.

Compact tension specimens with 50.8mm width were utilized for fatigue crack propagation tests according to ASTM E647. Specimens were 6, 12, and 24mm thick and were stress-relieved at 600°C for 1hr to exclude residual stress produced during machining. Fatigue tests was performed on Instron 8501 servohydraulic dynamic testing machine under a load ratio of 0.1 and a sinusoidal frequency of 10Hz in room temperature air. Crack length was optically monitored with a closed-circuit detection camera at a magnification of 50. In addition, elastic compliance method with a crack opening displacement (COD) gage was employed to measure the crack length. Fatigue precrack of 3mm in length was produced and then ΔK-decreasing tests were started from ΔK of 10MPam$^{1/2}$. The value of threshold was defined as the ΔK level corresponding to a crack propagation rate of 10^{-7}mm/cycle. Subsequently, ΔK-increasing tests were performed on the same specimens at constant load. Crack closure load was determined from a series of plots of load vs. COD at 1Hz taken just prior to each ΔK reduction using modified compliance method. It was defined as the inflection point where the load vs. COD curve began to deviate from the upper elastic unloading line [12].

RESULTS

Fatigue crack propagation results

The variations of crack propagation rate, da/dN, as a function of stress intensity range, ΔK, are presented in Figure 2. In general, crack propagation rates in Paris' region were insensitive to specimen thickness. However, near-threshold crack propagation rates decreased and ΔK_{th} increased for all microstructures with increasing specimen thickness. Figure 3 presents the crack propagation behavior of the SA106 Gr.C steel base before and after the spheroidization. After the spheroidization, the ΔK_{th} value of 24mm thick specimen decreased from 7.08MPam$^{1/2}$ to 6.44MPam$^{1/2}$, while that of 6mm thick specimen was nearly the same. It can be inferred that the effect of microstructural variation is more significant in thicker specimen.

In order to compensate for the variation in yield stress and to appreciate the real contribution from the effective grain size [13] alone, the variation of ΔK_{th} with the parameter, $\sigma_{ys} l'^{2}$ is plotted in Figure 4. The lines represent least-square fits to the data. More marked increase in ΔK_{th} with increasing value of $\sigma_{ys} l'^{2}$ can be seen. The values of ΔK_{th} increased monotonously with increasing thickness except for the SA106 Gr.C steel base in which, the values of ΔK_{th} were nearly the same for 12mm and 24mm thick specimens.

Crack closure behaviors

Table 3 summarized the fatigue threshold values such as ΔK_{th}, threshold stress intensity range, $K_{cl,th}$, crack closure stress intensity at threshold, and $\Delta K_{eff,th}$ effective threshold stress intensity range. For a given material, the values of $\Delta K_{eff,th}$ were independent on specimen thickness and the dependence of $K_{cl,th}$ on specimen thickness was similar to that of ΔK_{th}. In the SA106 Gr.C steel base, the values of ΔK_{th} and $K_{cl,th}$ for 24mm thick specimens decreased after the spheroidization, while they remained nearly the same for 6mm thick specimens. As effective grain size increased, the values of $K_{cl,th}$ increased at a fixed specimen thickness. From these, it can be inferred that the crack closure is mainly responsible for the effects of specimen thickness and microstructure on ΔK_{th}.

Fractography

Figure 5 shows the macroscopic fractographs of the fractured specimens for SA106 Gr.C steel base and 12% Cr steel. Oxide debris was observed at near-threshold region and is obviously related with oxide-induced crack closure. In 6mm thick specimen, oxide debris was observed only on the fracture surfaces of the SA106 Gr.C steel base and weld. As specimen thickness increased, crack fronts at near-threshold changed from a convex to a concave shape to crack propagation direction and thicker oxide debris was concentrated only at the central portion of specimens. However, the degree of concavity through thickness was lesser in 24mm thick specimens than in 12mm thick specimens. The other materials revealed the same trends. It can be inferred that an increase of plastic constraint at the crack tip due to increasing specimen thickness enhanced oxide-induced crack closure and modified the crack front shape.

Scanning electron fractographs of fracture surfaces at near-threshold region for the SA106 Gr.C steel base and weld are presented in Figure 6. Many asperities were observed at the central portion of the specimens, but not observed near the outer surfaces of specimens. They are observed only on both 12mm and 24mm thick specimens in the SA106 Gr.C steel base and on 24mm thick specimen in the weld. The asperities in the weld were small and closely distributed compared to those in the SA106 Gr.C steel base. As can be seen in Figure 7, after the spheroidization, the numbers of asperities were reduced and the size was decreased. Figure 8 shows a magnified fractography of the asperities. The hill and valley of the asperities were covered with dark oxide deposits. It can be deduced that the large asperities promoted oxide-induced crack closure. The distribution and the size of the asperities may be attributed to the difference in the grain size and the pearlite content.

DISCUSSION

Influence of specimen thickness

In the present study, it was found that ΔK_{th} was higher in thicker specimens regardless of the microstructures and the crack front at threshold was changed from a convex to a concave shape with increasing thickness. The thickness effect attributed to the crack closures can be explained with plastic constraint at the crack tip.

From the modified Dugdale model [14], cyclic plastic zone size, r_{cyclic}, and cyclic crack-tip opening displacement, $CTOD_{cyclic}$, are expressed such as

$$r_{cyclic} \propto \left(\frac{\Delta K}{\alpha \sigma_{ys}}\right)^2 \tag{1}$$

$$CTOD_{cyclic} \propto \frac{\Delta K^2}{\alpha \sigma_{ys} E} \tag{2}$$

where E is Young's modulus and α is a constraint factor that is 1 for plane stress and 3 for plane strain. In thin specimen, the stress state at the crack tip will vary less significantly along the crack front and the relatively larger plastic zone size near the outer surface leads to more plasticity-induced crack closure. The ends of the crack front at the surface will trail behind the major part of the advancing crack front. As a result, the slightly convex crack front shape would be obtained in 6mm thick specimen, as presented in Figure 6. However, the strain gradient at the crack tip will be higher and plane strain condition at the crack tip will be prevalent internally with increasing thickness. Under plane strain condition, r_{cyclic} and $CTOD_{cyclic}$ decreases significantly due to the plastic constraint effect compared to plane stress for a given ΔK. In this circumstance, the contribution of plasticity-induced crack closure at the outer surfaces would be relatively small compared to roughness-induced crack closure at the interior. Thus, effective stress intensity range, ΔK_{eff}, at the interior was lower than that at the surface and crack would still continue to grow at the surface after being arrested at the central portion of specimen. By prolongation of the fretting contact of the crack frank, the thick oxide debris would be obtained and thus ΔK_{th} increased.

Influence of microstructure

As the effective grain size increased, the thickness effect became more pronounced. Several investigators suggest that when the r_{cyclic} at a value ΔK_T becomes comparable to grain size, a transition from continuum-controlled striation crack growth to a crystallographically influenced faceted crack growth occurs.

$$r_{cyclic} \propto (\frac{\Delta K_T}{\alpha \sigma_{ys}})^2 \approx l \tag{3}$$

If the ΔK_T is approximately assumed in term of ΔK_{th} and rearranging Eq (3), it is seen that

$$\Delta K_{th} \propto \alpha \sigma_{ys} \sqrt{l} \tag{4}$$

As shown in Figure 4, the slopes, $\Delta K_{th}/\sigma_{ys} l^{1/2}$, which is related with plastic constraint at the crack tip were higher in thicker specimens. As plastic constraint at the crack tip increases, $CTOD_{cyclic}$ will significantly decrease for a given ΔK and roughness-induced and oxide-induced crack closure would be more operative in coarse-grained microstructure than in fine-grained microstructure at relatively higher ΔK. Therefore, as the effective grain size increased, the thickness effect became more enhanced.

The values of ΔK_{th} increased monotonously except for the SA106 Gr.C steel base. It seemed that the pearlite content influenced on the thickness dependence of threshold value. The different dependence of ΔK_{th} on specimen thickness for the SA106 Gr.C steel base and weld is related to pearlite content as shown in Figure 3 and Figure 4. The pearlite content of the weld was so low that ΔK_{th} increased monotonously with thickness like the SA508 Cl.3 and 12% Cr steels. However, the ΔK_{th} of the SA106 Gr.C steel base saturated at 12mm. Under plane strain condition, the shear deformation of pearlite will be difficult in plastic zone. The preferred path of a fatigue crack in ferrite-pearlite microstructure is through the ferrite or through pearlite colonies suitably oriented for fracture by shear deformation [15, 16]. However, pearlite colonies, which are not suitably oriented for fracture by shear deformation, would be branched and meandered under plane strain crack tip. Crack tip is not a single point but a line. Different parts of the crack front will find it easier or harder to advance, owing to the varying condition of the local microstructure along the crack front. It is considered that at threshold region, ΔK_{eff} at pearlite phase will be lower than that at ferrite phase by branching and meandering, so crack would still continue to grow preferentially through the ferrite phase

remaining ligaments of unfractured pearlite colonies. Then, the unfractured ligament would be failed by low-cycle fatigue process as shown in Figure 8 [17, 18]. Mismatching asperities would increase fracture surface roughness and thus ΔK_{th} increased. Therefore, as shown in Figure 7, the number and the size of asperities were significantly reduced, and ΔK_{th} decreased after the spheroidization of pearlite.

CONCLUSIONS

Based on microstructural point of view, the effect of specimen thickness on near-threshold fatigue crack propagation behavior of low carbon steels has been investigated. The following conclusions were obtained:

(1) Near-threshold crack rates decreased and threshold values increased with increasing specimen thickness regardless of the microstructures and the thickness effect became more pronounced as the effective grain size increased. The thickness effect was attributed roughness-induced and oxide-induced crack closures that were enhanced at the plastic constraint field.

(2) Pearlite affected the dependence of ΔK_{th} on specimen thickness. It was confirmed by the spheroidization of pearlite that pearlite retarded effectively near-threshold crack propagation by promoting roughness-induced crack closure under plane strain condition.

REFERENCES

[1] Elber, W., Eng. Fract. Mech. 1970, 2, 37-45
[2] Suresh, S., Zamiski, G. F., and Ritchie, R. O., Metall. Trans. 1981, 12A, 1435-1443
[3] Liaw, P. K., Leax, T. R., and Logsdon, W. A., Acta Metall. 1983,31, 1581-1587
[4] Minakawa, K. and McEvily, A. J., Scr. Metall. 1981, 15, 633-636
[5] Gray, G. T., Williams, J. C., and Thompson, A. W., Metall. Trans. 1983, 14A, 421-433
[6] Bathias, C., Fatigue Eng. Mater. Struct. 1981, 4, 1
[7] Mingda, G., Chuanfu, D., Wei, Z., and Minggao, Y., Fatigue 84, Proceedings of an International Conference, E.M.A.S., 1985, Vol.1, 287-295
[8] Radon, J. C., Fatigue Threshold, Proceedings of an International Conference, E.M.A.S., 1981, 1, 113-132
[9] Musuva, J. K. and Radon, J. C., Materials, Experimentation and Design in Fatigue, Proceedings Fatigue '81, 1981, 106-116
[10] Romaniv, O. N., Tkach, A. N., and Lenets, Y. N., Fatigue Fract. Eng. Mater. Struct. 1987, 10, 203-212
[11] Tokaji, K., Ando, Z., and Nagae, K., J. Eng. Mater. Tech. 1987, 109, 86-91
[12] Donald, J. K., Mechanics of Fatigue Crack Closure, ASTM STP 982, 1988, 222-229
[13] Yoder, G. R., Cooley, L. A., and Crooker, T. W., Fatigue 84, Proceedings of an International Conference, E.MA.S., 1985, Vol.1, 351-360
[14] J. C. Newman, ASTM STP 748, 1981, 53-84
[15] K. W. Burns and F.B. Pickering, J. Iron Steel Inst., 1967, 202, 899
[16] L. E. Miller and G. C. Smith, J. Iron Steel Inst., 1970, 208, 998
[17] W. W. Gerberich and N. R. Moody, Fatigue Mechanisms, Proceedings of an ASTM-NBS-NSF symposium, ASTM STP 675, 1979,292-341
[18] L. Edwards and J. W. Martin, Metal Science, 1983, 17,511

Table 1Chemical compositions of the tested materials (wt%)

element	C	Mn	Si	Ni	Cr	Mo	P	S	V	Nb
SA106 Gr.C	0.19	1.22	0.27	0.11	0.05	0.03	0.009	0.007	0.004	-
Weld	0.073	1.44	0.83	0.007	0.02	0.03	0.015	0.017	0.007	-
SA508 Cl.3	0.21	1.36	0.25	0.92	0.21	0.49	0.007	0.002	0.005	-
12% Cr	0.17	0.68	0.22	0.55	10.81	0.90	0.009	0.002	0.19	0.05

Table 2 Room temperature tensile properties with microstructural characteristics

Material	l (μm)	pearlite volume fraction	σ_{ys} (MPa)	σ_{uts} (MPa)	e_u (%)
SA106 Gr.C	25	24	335(301*)	556(512*)	33(36*)
Weld	12	8	396	542	35
SA508 Cl.3	5	-	446	589	29
12% Cr rotor	0.4	-	784	907	19

l: effective grain size * : spheroidized

Table IV-2 Fatigue threshold results

Material	B(mm)	ΔK_{th}(MPa√m)	$K_{el,th}$(MPa√m)	$\Delta K_{cr,th}$(MPa√m)
SA106 Gr.C	6	5.38	2.39	3.58
	12	7.05	4.07	3.76
	24	7.03	4.43	3.38
Weld metal	6	5.15	2.56	3.16
	12	6.55	3.59	3.69
	24	7.08	4.29	3.58
SA508 Cl.3	6	4.66	1.88	3.29
	12	5.75	2.88	3.51
	24	6.05	3.05	3.67
12% Cr steel	6	4.50	0.98	4.02
	12	5.28	1.50	4.37
	24	5.59	1.88	4.33

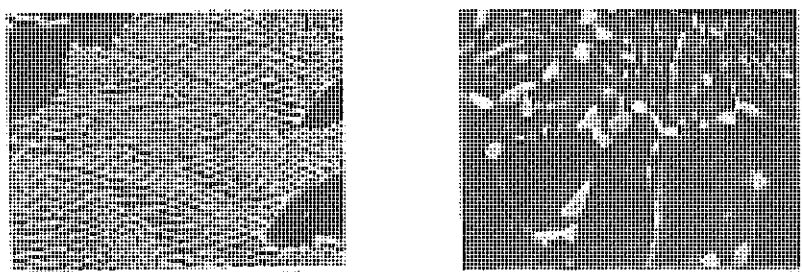

Figure 1 SEM micrographs of SA106 Gr.C base; (a) before and (b) after the spheroidization

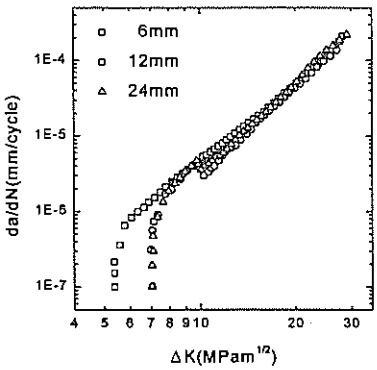

(a) SA106 Gr.C base

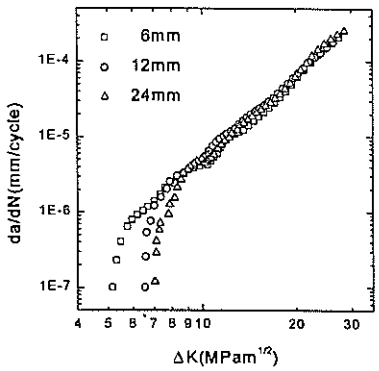

(b) Weld

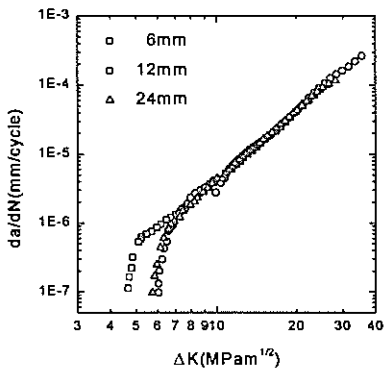

(c) SA508 Cl.3

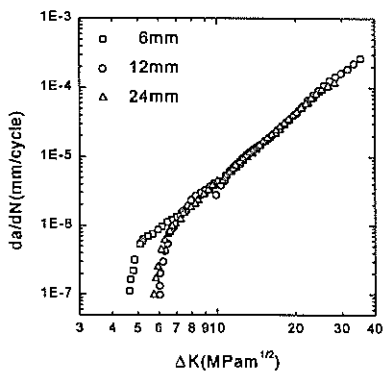

(d) 12% Cr steel

Figure 2 Fatigue crack propagation behaviors

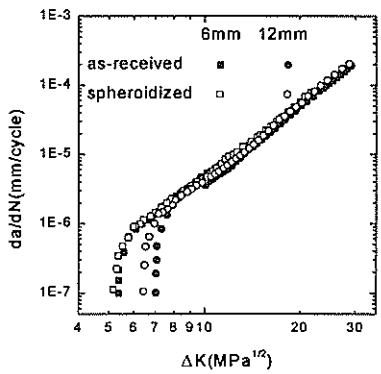

Figure 3 Fatigue crack propagation behavior of SA106 Gr.C base

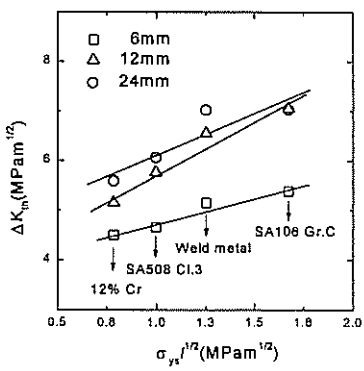

Figure 4 ΔK_{th} as a function of $\sigma_{ys} l^{1/2}$

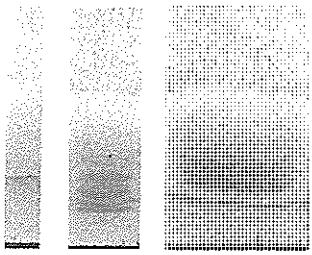

Figure 5 Macro-fractographs of SA106 Gr.C base

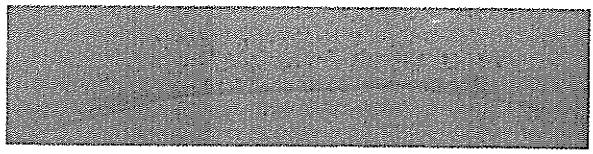

(a) SA106 Gr.C base

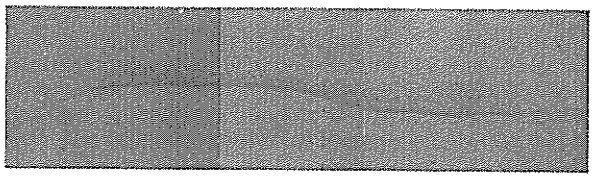

(b) weld

Figure 6 SEM fractographs at threshold for 24mm thick specimens: (a) SA106 Gr.C base and (b) weld

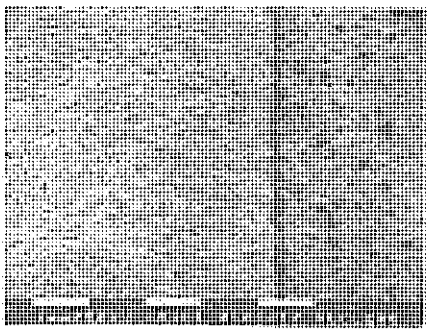

(a)

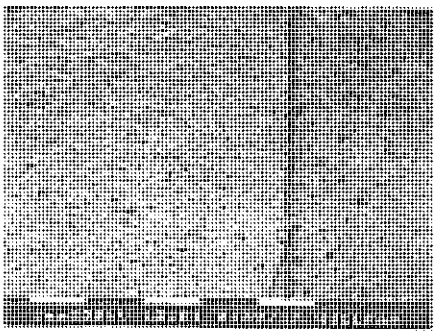

(b)

Figure 7 Change in the distribution and the size of asperities in 24mm thick specimens for SA106 Gr.Csteel : (a) before and (b) after the spheroidization

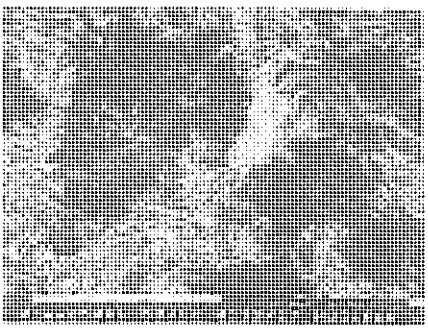

Figure 8 Magnified SEM fractograph showing large asperities